processes

Review

Gravitational Surface Vortex Formation and Suppression Control: A Review from Hydrodynamic Characteristics

Gaoan Zheng [1], Zeheng Gu [2,3], Weixin Xu [2,4], Bin Lu [2,3], Qihan Li [2], Yunfeng Tan [2,3], Chengyan Wang [2,3] and Lin Li [2,3,4,*]

1 College of Mechanical and Automotive Engineering, Zhejiang University of Water Resources and Electric Power, Hangzhou 310018, China
2 College of Mechanical Engineering, Zhejiang University of Technology, Hangzhou 310014, China
3 Key Laboratory of Special Purpose Equipment and Advanced Processing Technology, Ministry of Education & Zhejiang Province, Hangzhou 310014, China
4 State Key Laboratory of Fluid Power and Mechatronic Systems, Zhejiang University, Hangzhou 310027, China
* Correspondence: linli@zjut.edu.cn

Abstract: The energy-conversion stability of hydropower is critical to satisfy the growing demand for electricity. In low-head hydropower plants, a gravitational surface vortex is easily generated, which causes irregular shock vibrations that damage turbine performance and input-flow stability. The gravitational surface vortex is a complex fluid dynamic problem with high nonlinear features. Here, we thoroughly investigate its essential hydrodynamic properties, such as Ekman layer transport, heat/mass transfer, pressure pulsation, and vortex-induced vibration, and we note some significant scientific issues as well as future research directions and opportunities. Our findings show that the turbulent Ekman layer analytical solution and vortex multi-scale modeling technology, the working condition of the vortex across the scale heat/mass transfer mechanism, the high-precision measurement technology for high-speed turbulent vortexes, and the gas–liquid–solid three-phase vortex dynamics model are the main research directions. The vortex-induced vibration transition mechanism of particle flow in complex restricted pipelines, as well as the improvement of signal processing algorithms and a better design of anti-spin/vortex elimination devices, continue to draw attention. The relevant result can offer a helpful reference for fluid-induced vibration detection and provide a technical solution for hydropower energy conversion.

Keywords: gravitational surface vortex; hydrodynamic characteristics; vortex-induced vibration; hydropower energy conversion; hydropower station

check for updates

Citation: Zheng, G.; Gu, Z.; Xu, W.; Lu, B.; Li, Q.; Tan, Y.; Wang, C.; Li, L. Gravitational Surface Vortex Formation and Suppression Control: A Review from Hydrodynamic Characteristics. *Processes* **2023**, *11*, 42. https://doi.org/10.3390/pr11010042

Academic Editor: Udo Fritsching

Received: 6 December 2022
Revised: 21 December 2022
Accepted: 22 December 2022
Published: 25 December 2022

1. Introduction

Due to the worsening of natural environments, countries in the world have placed considerable emphasis on the usage and development of cleaner energy [1,2]. Hydropower is widely applied in power system generation and grid stabilization due to its unparalleled flexibility and energy storage advantages. In 2020, hydropower will generate approximately 16% of global electricity. The International Energy Agency (IEA) stated that global hydropower generation would have to treble from anticipated levels to achieve global net-zero emissions by 2050. In addition to electricity generation, the reliability of power grid systems is becoming increasingly important [3]. Due to their dual characteristics of high responsiveness, pumped-storage power stations play a significant role in balancing the power load.

Traditional hydro turbines require the damming of rivers to generate large water heads. Such structures can be dangerous and expensive to build [4]. The low-head turbine offers advantages of operating at low heads, lacking geographical and topographical constraints. The output of a low-head turbine is comparable to that of a regular turbine, and it is commonly utilized in hydropower system building.

The turbine in low-head hydroelectric power plants runs near the liquid surface, with a little space between runners and channel entrances. The interaction of gas and liquid at upper reservoirs produces complex physical phenomena such as a surface vortex and pressure fluctuation under gravity. It affects the flow stability and turbine performance of the turbine inlet, making synchronization with the power grid difficult when the hydropower station is started [5–7]. The gravitational surface vortex formed during the operation of the hydropower station is shown in Figure 1. As the turbine unit drains, the powerful gravitational surface vortex may draw floating debris and air into the inlet, causing irregular pulsing pressure. The air entrainment creates cavitation and adds a pulsing load to the nozzle connection mechanism, increasing the risk of hydraulic-equipment damage [8–10]. In view of these omitting problems, surface vortexes have been extensively studied in the last 50 years—particularly in the field of hydraulic engineering—and effective anti-vortex measures have been implemented to actively detect and control vortex formation at turbine inlets.

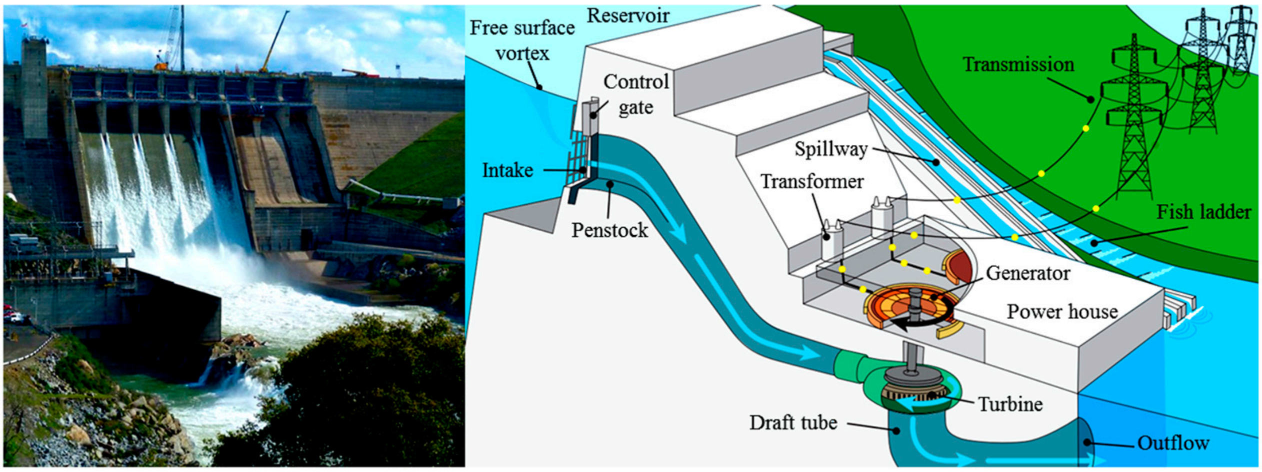

Figure 1. Gravitational surface vortex generated at the hydropower station [5].

The gravitational surface vortex is a three-dimensional and multiphase phenomenon. It is a nonlinear dynamic issue involving multiphase coupling, heat/mass transfer, pressure pulsation, and other effects [11–14]. There are currently no well-developed theoretical models for an accurately quantified discussion of its generation mechanism, multi-field coupling transport characteristics, and impact vibration characteristics. Limited local characteristics can only be obtained under ideal assumptions or in combination with experimental studies [15–22]. The interfacial morphology and flow pattern are nonlinear due to the surface vortex's characteristics, such as its three-dimensional instability, turbulence, and spatio-temporal multi-scale coupling [23–34]. It makes it difficult to accurately characterize physical variables like the vortex scales, vorticity features and streamlining evolving [35–45]. Thus, studying the formation and evolution of gravitational surface vortices and controlling them is a critical topic for improving the performance and stability of water-turbine units.

This paper systematically presents the hydrodynamic features of the gravitational surface vortex and the development of its research. We outline and assess the hydrodynamic characteristics and state detection and prospect their future research directions. Our research can be used as a theory reference for hydropower researchers working on surface-vortex modeling, flow-pattern evolution mechanisms, vortex-induced vibration, and other topics with a promising future in some industrial domains, such as hydroelectric energy conversion and the development of low-emission energy systems.

2. Dynamic Evolution Characteristics of Gravitational Surface Vortex

2.1. Pumping Effects of the Ekman Layer

For a rotating source-sink system, a surface vortex is prevalent in nature and technology, and it frequently generates intriguing flow shapes with the Ekman boundary layer. The critical aspect is that vortex motions will become nonlinear since they are viscous frictions at interfaces and transfer characteristics.

As a crucial method of analyzing boundary layers, Ekman's theories have been extensively applied in oceanography [46–50], meteorology [51], engineering fluid computation [52], and other disciplines. Andersen [53] investigated the dynamic evolution characteristics of the Ekman layer and found the Ekman upwelling flow phenomenon. In Figure 2, Chen [54] obtained single-celled structures with upwelling zones and found the fluid particle moved to the center nozzle via the Ekman layer [53]. The flow pattern and scale connection with distinct shear layers were found in the Ekman boundary layer, but the flow field structure, such as a Taylor column, may produce a more complicated flow layer structure. As a result, the impact of a more extensive range of flow conditions on the Ekman layer for the surface vortex from laminar to turbulent states may be examined.

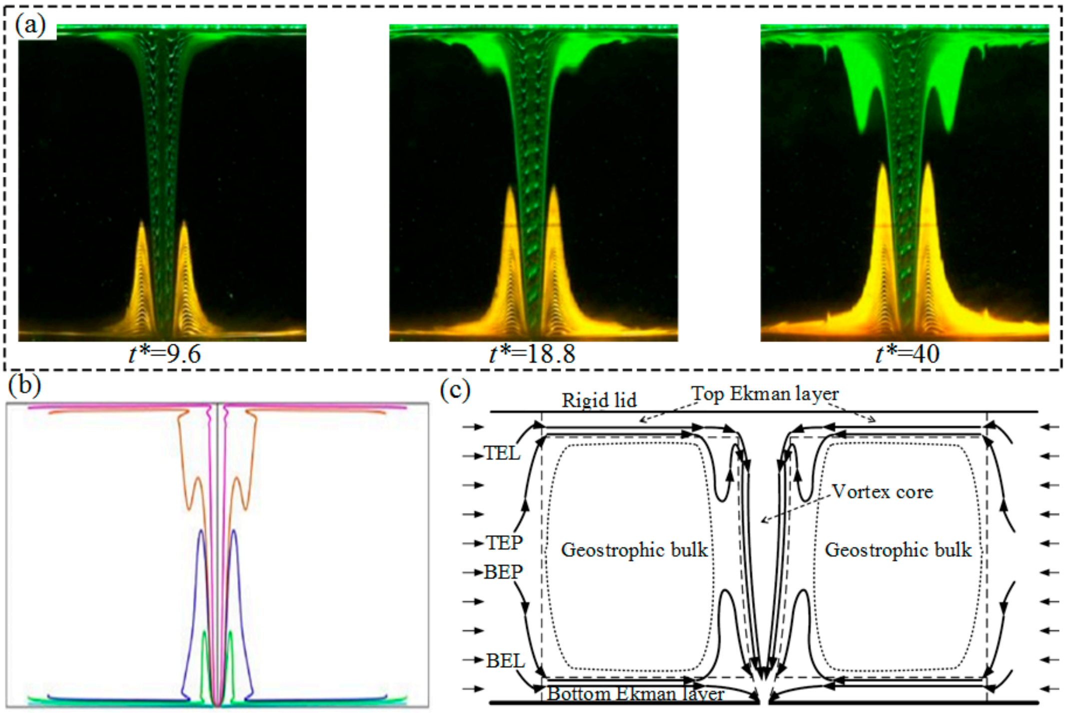

Figure 2. The evolution process of the Ekman layer (t^* represents the normalized time). (**a**) Flow visualizations of steady vortexes. (**b**) Streamline on meridional r–z planes. (**c**) Flow pattern sketch. (Reprinted with permission from Ref. [54]. 2013, Cambridge University Press).

Son [55] investigated the air-core phenomena with a cylindrical tank and explored its formation process. Due to centrifugal instabilities, Taylor vortices developed along the side wall (Figure 3a), progressively increasing their volume in the tank. Park [56] looked at the Taylor and Ekman vortices and how they interact and found that axially spinning-downward flow structures accessed the Taylor-vortex ring (Figure 3b), which demonstrated the effects of Ekman effects on vortex cores. Yokoyama [57] observed that vortexes take on the two cell structures with transport and ascending characteristics. Kim [58] investigated the generating course of gravitational-surface vortexes (Figure 3c) and observed that bubble flows and separating processes of the eddy vortex are affected by the Ekman layer, which illustrates that the Ekman layer appears to impact vortex production considerably.

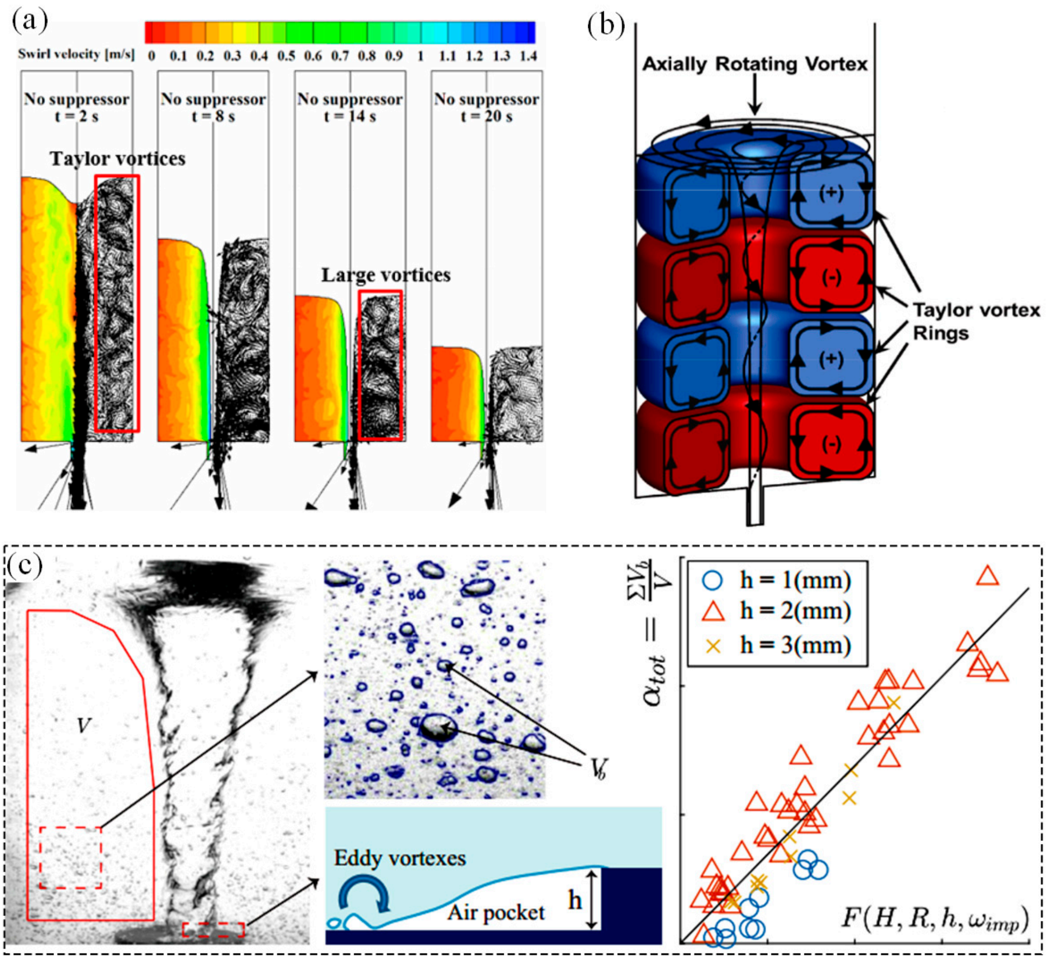

Figure 3. Turbulence structures evolution of vortex flow fields [55,56,58]. (**a**) Distributions of swirl velocity. (Reprinted with permission from Ref. [55]. 2018, Springer Nature). (**b**) Schematic image of the vortex interaction. (Reprinted with permission from Ref. [56]. 2011, Elsevier). (**c**) Total void fraction. (Reprinted with permission from Ref. [58]. 2021, Elsevier).

In order to better understand the physical factors that affect vortex flow, the Ekman layer suction idea in a theoretical model might be beneficial in examining the gravitational vortexes. It is theoretically possible to examine the gravitational vortexes using a precise and reliable physical model. Further vortex theoretical investigation on transporting impacts, cross-scale vortex-cluster evolution, measured boundary layers, and other crucial dynamics elements was needed based on the Ekman-layer theories.

According to the above literature, the nonlinear turbulent features of Ekman layers were not disclosed. It is challenging to undertake analytical calculations to determine the thicknesses of Ekman layers, and developing models suited for core regions (which are inadequately anticipated by present models) was difficult for the theoretical study [56]. The energy transfer of partial vortices, vorticity aggregating and dissipating courses, and Ekman layer's trans-scale suction and transport phenomena are yet unknown for multiphase viscous vortices.

2.2. Heat/Mass Transport of Vortex Flow

The transport effect of large-scale vortices contributes to transport mass, kinetic energy, and energy across surface vortex phases driven by a specific potential field (temperature field, pressure field, gravity field, etc.). These will cause significant heat and mass transfer, increase small-scale vortex movement, and generate a complicated multi-field coupling phenomenon.

More and more researchers are studying the heat/mass transmission process. Lamont [59] examined viscous dissipative vortices with a small vortex model. Low-energy vortices were discovered to accelerate vortex mass transfer at various sizes by increasing the mixing degrees of giant vortexes. Morales [60] investigated the momentum and heat transmission of the vortex and discovered that temperature gradients caused by wall heat losses supplied buoyancy forces significant enough to impact liquid motion. The buoyancy force raised critical heights of vortex generation and suspended solids suction. Aravind [61] looked into the transfer mechanisms of the compressible vortex flow field (Figure 4a). The vortices created by the lateral provide a rapid mass transfer boost at the vortex generators (x/B = 0.3) (Figure 4b). The secondary flow appears to produce the intense temperatures and density differential, improving the mass transfer process between surrounding surfaces. Furthermore, the horseshoe vortices formed (Figure 4c) near the boundary contributed to this amplification.

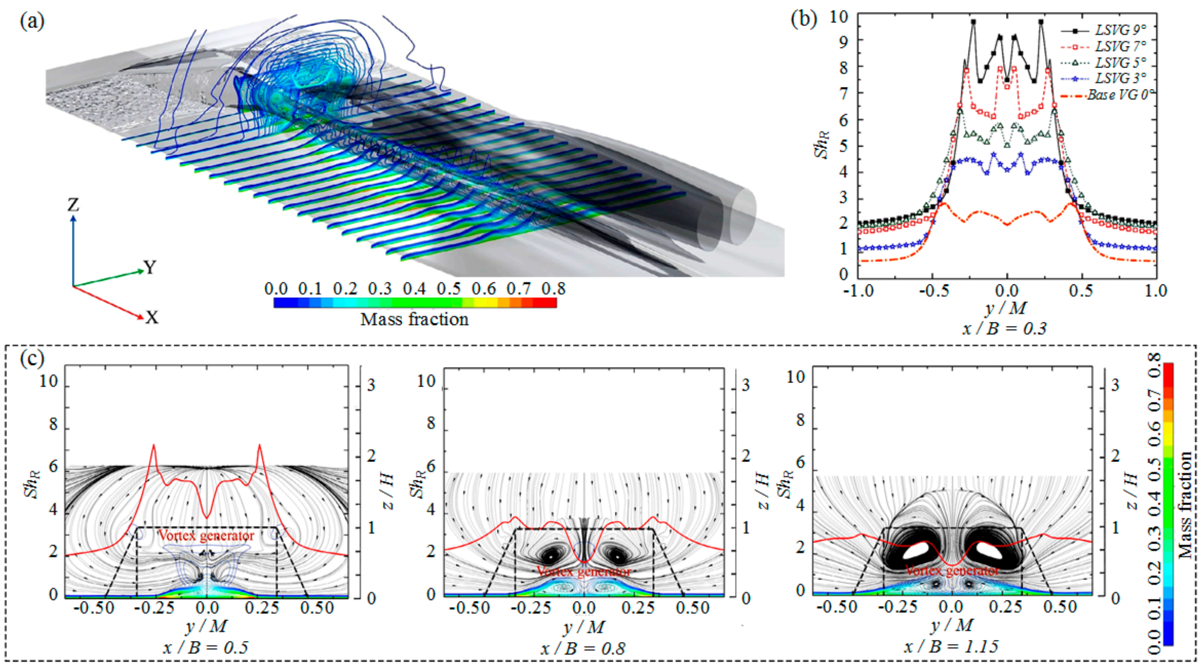

Figure 4. Mass transfer process of the compressible vortex flow field. (**a**) Species profiles with mass fraction. (**b**) Mass transfer profiles at x/B = 0.3. (**c**) Streamlines of species mass fraction. (Reprinted with permission from Ref. [61]. 2017, Elsevier).

Nazir [62] investigated the effects of temperatures on gas-core development computationally and empirically in recent years. The findings revealed that the air core becomes more potent when the temperature rises, resulting in a decrease in fluid viscosity. Tan [63] examined the intrinsic link between initial velocities and the mass transfer process using the multiphase-vortex models. The particle pumping of the flow field revealed that vorticity transition occurred during this phase, which aided in the mass transfer of various turbulent vortices. Monji [64] investigated the influence of water temperatures on vortex-core lengths and found that vortex-core lengths rise as temperatures are greater. The temperature played a vital role in affecting vortex flows.

Although substantial progress has been achieved in the number of surface vortex heat/mass transfers, most studies are confined to two-phase flow at low Reynolds numbers and overlook the effect of the Ekman layer on the heat/mass transfer process. It is critical to continue to investigate the multi-scale modeling technology of surface vortexes, which combines variable magnetic field, thermal radiation, and other external factors; accurately measure the vortex gas core formation process; and study the transmission features of multi-physical field coupling driven by thermal/magnetic potential fields.

2.3. Gravitational Surface Evolution and Flow-Pattern Tracking

Due to interfacial suction forces and viscous frictions, the interfacial shapes and flow-patterns display nonlinear properties in vortex formation courses. It is difficult to fully quantify the multi-dimensional dimensions of vortex core size, shape, and flow trajectory.

Under constant input and exit conditions, water-model experimental research is used to study the critical vortex heights, gas-core evolution, and speed distributions. Tahershamsi [65] used the experimental approach to investigate the hydrodynamic behavior of vortexes and obtained an air-core vortex (Figure 5a), and found that the gas core looked to be an air tube at lower Reynolds numbers. Ruan [66] looked into the dynamic evolution of the vortex core, observing four stages of its interface shape and comparing the data to the numerical model (Figure 5b). Their findings, however, were confined to the development of the interface at the surface vortex's lower Reynolds number. Mulligan [67] investigated a Taylor-Couette vortex system to explore the stationary vortex with increasing Reynolds numbers (Figure 5c). At the centrifugal effects of wall-bounded vortexes, the instability state was observed.

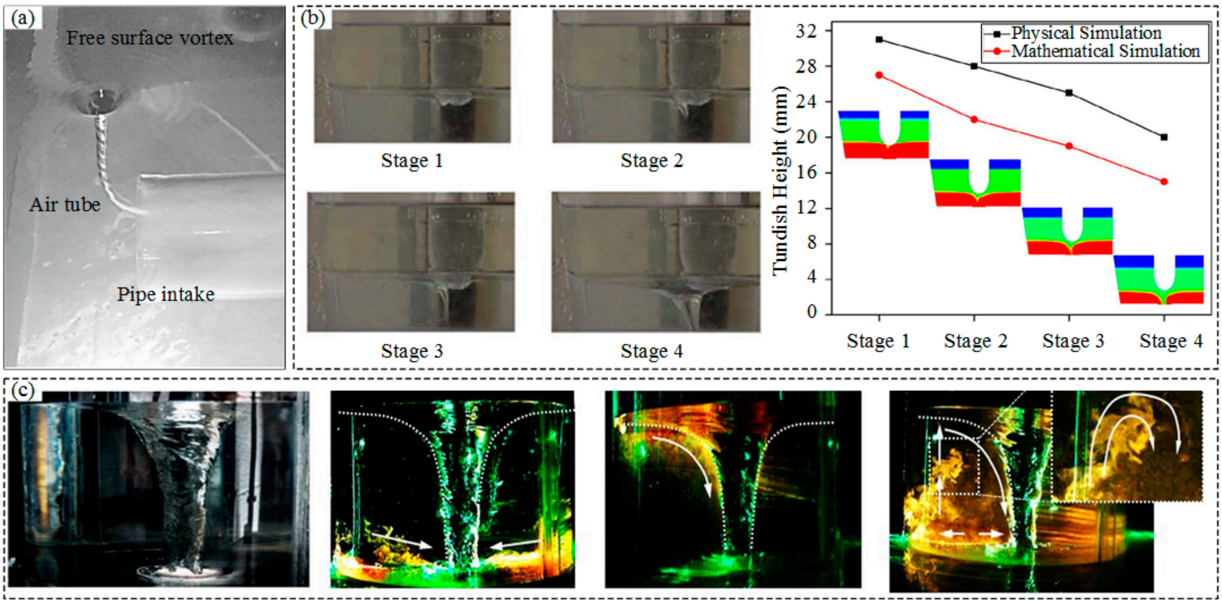

Figure 5. The evolution process of the gravitational surface. (**a**) Air-core vortex. (Reprinted with permission from Ref. [65]. 2018, Springer Nature). (**b**) Four stages of vortex formation. (Reprinted with permission from Ref. [66]. 2020, Springer Nature). (**c**) Steady vortex with a high Reynolds number. (Reprinted with permission from Ref. [67]. 2018, Springer Nature).

Son [68] constructed the simulations of the vortex gas-core phenomenon and looked at the vortex dynamic evolution (Figure 6), and could effectively duplicate flow patterns like spiral gravitational surface waves in the ring Taylor vortex core. The dynamics of the gravitational surface vortex derived by Wu [69] showed that its circulation ranged from low (t = 4160 d/V) to high (t = 4240 d/V). Yang [70] obtained the oil-phase eddy current field with numerical models, revealing fluid field structures and evolving processes of three-phase vortexes. Tan [71] presented the turbulence models for the gas–liquid vortexes that effectively replicated their vital penetrating processes and demonstrated the transition laws of gas and liquid interfaces.

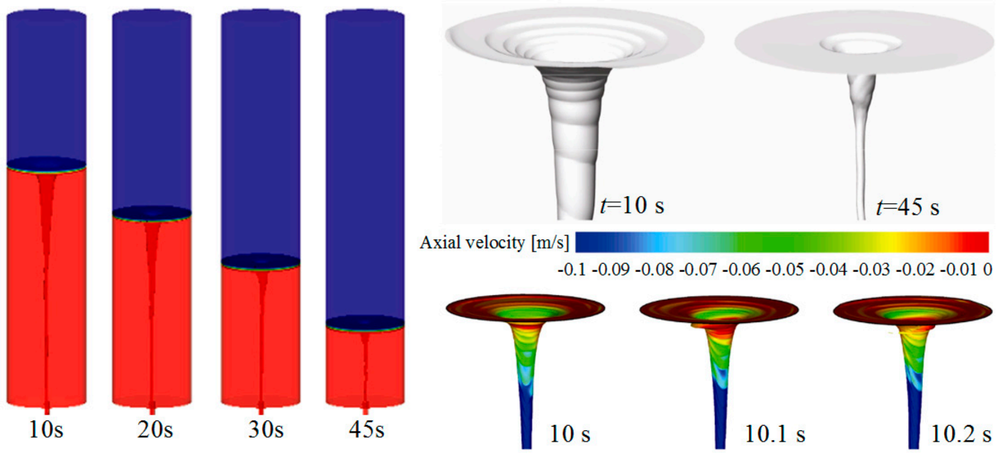

Figure 6. Evolving course of the free surface vortex. (Reprinted with permission from Ref. [68]. 2015, Springer Nature).

The surface vortexes show two-phase or multiphase flows with complicated and unpredictable moving features. The interactions of mediums with diverse qualities produce momentum, mass, and energy transmission mechanisms [71]. However, most research overlooked interphase slip across different fluid media, resulting in a loss of accuracy in two-phase transition interface simulations. As a result, improving numerical methods, higher-precision measurement experiments, simulation accuracy of multiphase interfaces, and achieving accurate surface vortex simulation is critical.

The flow patterns of particles propelled by the gravitational surface vortex were investigated by Duinmeijer [72,73]. The particle was discharged at the tank's surface, where it was grabbed by the vortex core and moved downhill after rotating (Figure 7a). After 7~8 s, the granule was nearly motionless at the z direction and rotating. When compared to the radial speed (<1.5 m/s), the z-direction velocities (Figure 7b) were significantly low (<0.15 m/s). The particle's acceleration (Figure 7c) grew progressively after release, and its value reached more than 100 m/s^2 and then decreased. Although flow-pattern evolutions of multi-particles in a strong turbulent vortex evolution process have been observed at low Reynolds numbers, the flow pattern evolution of single-particle vortex flow fields has not been observed. As a result, more research into high-precision vortex particle-flow measuring technologies is required.

Xie [74] used enhanced interphase slip moment techniques to examine the Rankine vortex's development. If the particle radius is high enough, the slip effect is exacerbated, resulting in flow instability. Son [68] observed vorticity distributions and streamlines at an 18 s time and inferred that intensive, axial flows in the container impacted Taylor vortexes and induced the vortex structure's temporal progression to be chaotic (Figure 8a). Li [75] examined the particle flow pattern in recent years, as shown in Figure 8b. The particle propelled by the vortex will consume much turbulence energy, lowering the energies of the entire flow field. Mulligan [67] confirmed the same results for the sizes and amount of growth of the vortices, as illustrated in Figure 8c. Ruan [66] looked at the clockwise and anticlockwise rotations (Figure 8d) and found a counterclockwise vortex at the outlet. It was found that the speed values of the flow pattern were higher near the outlets, causing the outlets to produce a vortex.

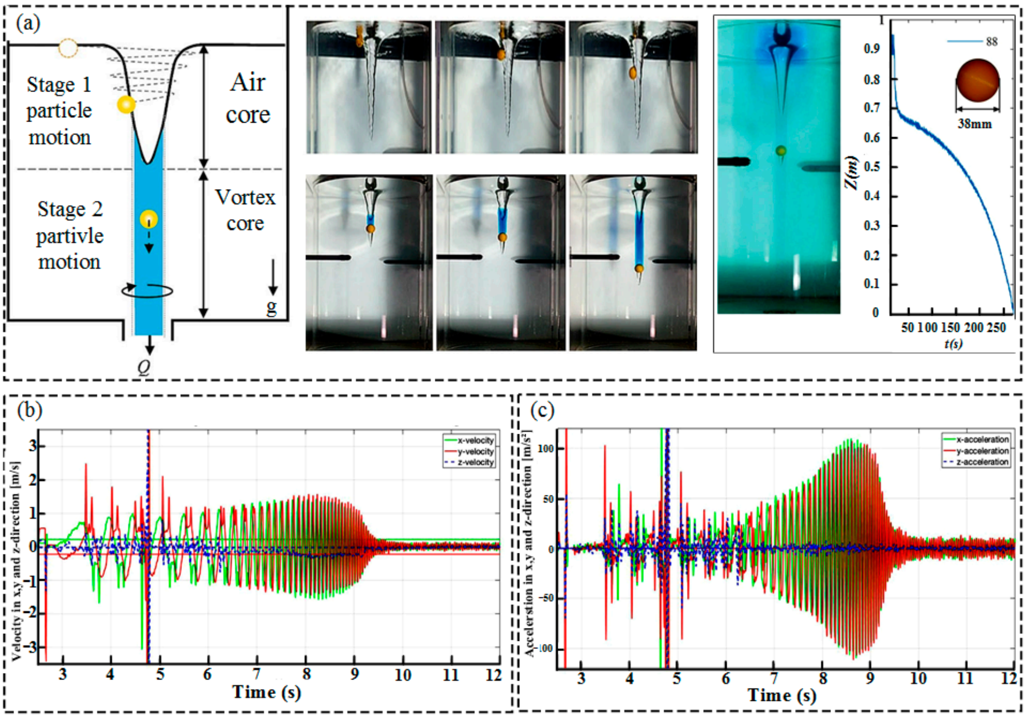

Figure 7. Particle motion is driven by surface vortex. (**a**) Particle motion. (**b**) x-y and z velocities. (**c**) Acceleration in x, y, and z directions. (Reprinted with permission from Ref. [73]. 2019, Springer Nature).

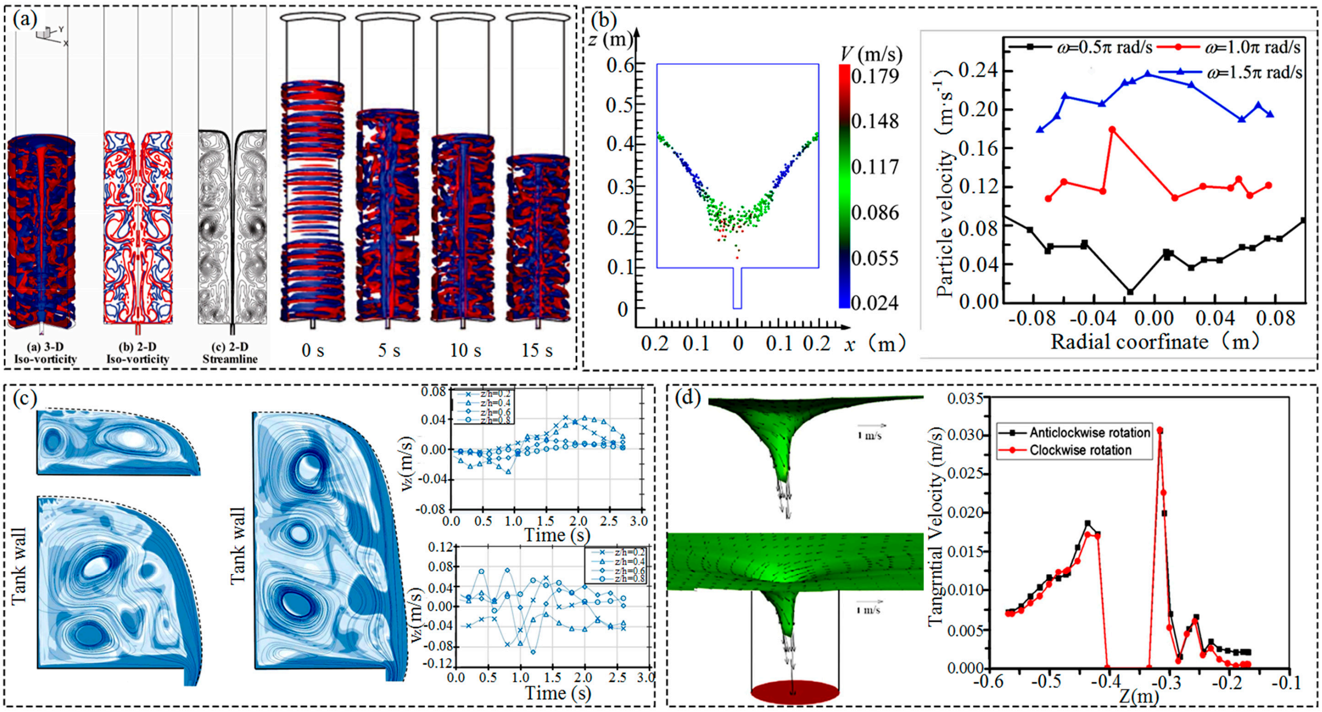

Figure 8. Flow patterns of the surface vortex [66–68,75]. (**a**) Vorticity distribution. (Reprinted with permission from Ref. [68]. 2015, Springer Nature). (**b**) Particle velocity. (Reprinted with permission from Ref. [75]. 2019, Elsevier). (**c**) Flow field streamlines. (Reprinted with permission from Ref. [67]. 2018, Springer Nature). (**d**) Flow patterns with a different rotation. (Reprinted with permission from Ref. [66]. 2020, Springer Nature).

According to the above literature, it can be found that the dynamic track techniques of vortex flow patterns mainly analyzed the evolving laws of two-phase vortexes. In contrast, flow-pattern analyzing methods oriented to multiphase vortexes were not clear [76]. As the particle size of solid particles is typically much smaller than the size of the computing grid, numerical stability at gas–liquid interfaces is a fundamental challenge for the numerical modeling of the solid particle phase; further research into how to increase numerical stability is needed. Furthermore, the impact of form factor, density, size, and other physical features of solid particles on gravitational surface vortex transport should be investigated further [77,78].

2.4. Vorticity Aggregation and Dissipation

The fluid energy release causes the suction course of surface vortexes, and its essence is the dissipation and aggregation of the turbulent vortex. Turbulence is caused by vortices nesting at various spatial and temporal scales. Energy is transported and changed at different sizes, and vortices at different scales exhibit self-similarity features [79,80].

Song [81] studied the formation course of surface vortexes in nuclear power plants (Figure 9a). The development rule of vortex intensity $I_s = \int_A S dA_h$ was studied, where S was the swirling strength computed via velocities and A_h was the horizontal circular slice. As the radius surpassed 0.0045 m and the dimensionless z/h value was modest, the I_s valve grew slowly with radius (Figure 9b). The swirling strength distribution was calculated based on the critical radius above in Figure 9c. It was found that the vortex intensity was centered in the gas–liquid mixed zone encompassed by the blue line and was more robust in the lower position. The mixing zone had a high speed and was affected by the exhaust port's suction, resulting in the highest vortex strength near the nozzle.

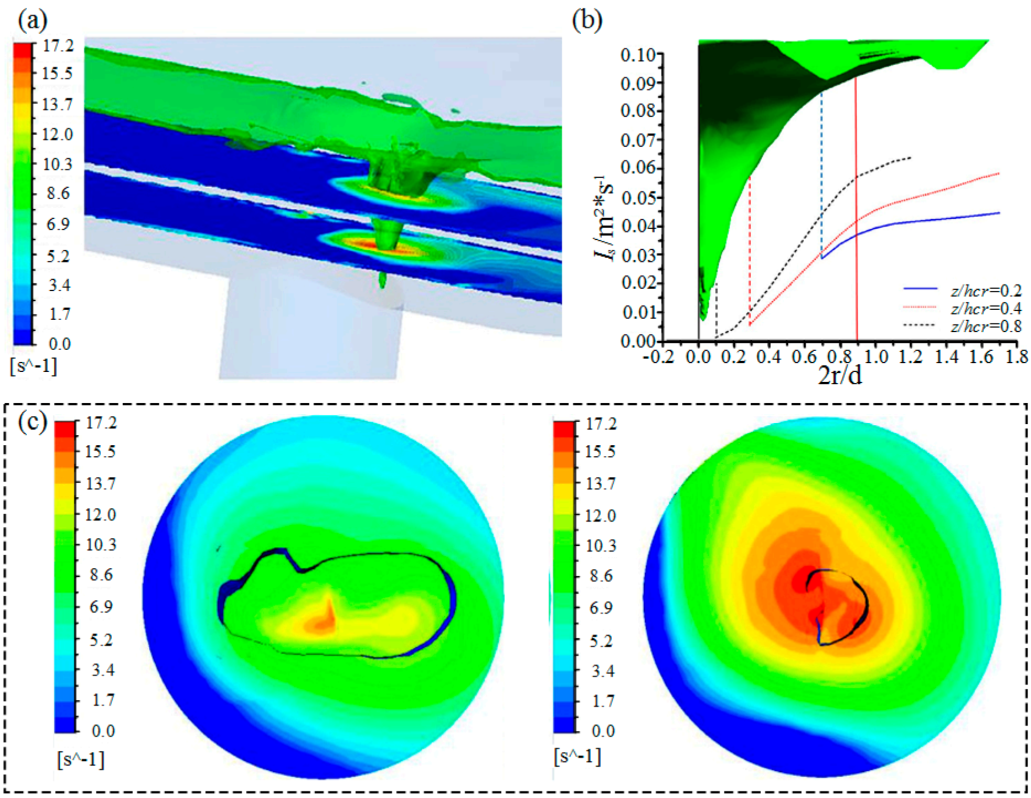

Figure 9. The dynamic evolution process of vortex intensity. (**a**) Swirling strength at different positions. (**b**) Vortex-intensity (I_s) curve. (**c**) Swirling-strength contour. (Reprinted with permission from Ref. [81]. 2018, Springer Nature).

Naderi [82] investigated the influence of the flow structures of the gas-core vortexes and found flow structures of mixing zones due to vortexes and closer flows interacting

(Figure 10a). The closer flow approached the vortex and generated turbulence mixed zones before being sucked into the secondary vortex upstream. The partial structure broke down into two small horizontal vortices vortex pairs at t = 4 s (Figure 10b). Then, the vortex pairs joined into the small coherent eddy at t = 8 s (Figure 10c). Decomposition and aggregation of turbulent vortices occurred because the secondary vortex spinning core was erratic, fluctuating in intensity and location. Tan [43] created the PIV experiment platform to explore the vortex suction processes. The vorticity takes on an aggregation tendency around the front end, revealing the vortex potential and kinetic energy transfer process.

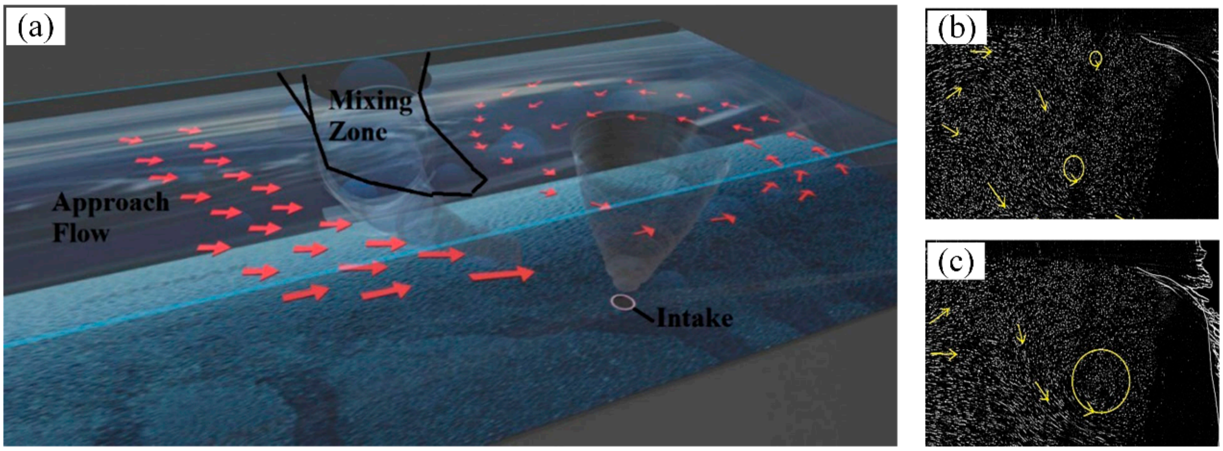

Figure 10. The evolution process of local vortices. (**a**) Diagram of vortexes, mixed zones, and closer flows. (**b**) Instantaneous streak line at t = 4 s. (**c**) Instantaneous streak line at t = 8 s. (Reprinted with permission from Ref. [82]. 2019, Springer Nature).

Based on the findings, it is necessary to continue investigating gravitational surface vortex energy transition dynamics modeling techniques, particularly the complex three-phase flow coupling modeling methods that take into account the solid particle phase, and to quantitatively analyze the internal relationship between flow pattern transition and vortex cluster energy evolution during vortex formation under turbulent conditions.

The ever-evolving vortex flow field made a quantitative investigation of vorticity aggregation and dissipation mechanisms difficult, especially at higher rotation speeds. Even though macroscopic turbulence intensity increases as circumferential speed increases, turbulence mixing and transfer speeds of various vortexes were unknown. Furthermore, the position of vortices had a random and nonlinear quality, which is related to some features such as turbulence disorders, disturbance speed, and vortices transferring course at various scales [83–85]. It is vital to explore energy evolution models of the surface vortexes and combine high-precision 3D vortex experimental models to verify the precision of the modeling methods.

2.5. Pressure Pulsation Phenomenon

According to related research, once the vortexes reach the pumps, they can damage their operating stability, cause vibrations and noises, accelerate bearing wear, and perhaps exacerbate blade cavitation. Owing to pump rotations and the sump geometry, the fluid fields have complex flow variations, notably between pumps and rear walls of closed sumps. The size and number of air bubbles sucked by the vortex will result in intense pressure pulsation.

Qian [86] studied the dynamic process of air entrainment and found that the dimple initially emerged on the surface and extended vertically towards the floor before moving up the intake pipe. The above phenomena demonstrated that the static pressure was lower than the pressure outside the vortex. According to the energy conservation law, when water starts to flow, there is a pressure differential between the gravitational surface and the intake pipe's entry. Air was entrained into the intake pipe when the pressure difference became significant. The pressure differential was a major factor in air entrainment.

Skerlavaj [87] studied the influence of pressure difference on air entrainment and found that vertical pressure gradients in the vortex core were insufficient, resulting in a shorter vortex gas-core length. Ezure [88] employed PIV measurement and velocity distribution attribute to identify the quantitative relationship between circulations, vertical seed gradients, and core lengths. It was found that the pressure-decrease index αΓ∞2 could evaluate time-series evolution behaviors of gas-core lengths. This approach using local quantities may remove the impact of experimental geometry and be applied to a wide range of geometries.

Zhang [89] found the pressure pulsation evolution by experimentally studying the evolving course of roof-attached vortexes, as shown in Figure 11. During the initial state of surface vortexes, pressures sited at P8 and P9 fell; however, the pressures of monitoring points (P4, P7, and P10) had no considerable variation. A surface vortex was more common at the P8 and P9 points. The frequency and pressure-pulsation coefficient C_p value of the vortex was not significantly different from the no-vortex situation. The typical frequencies were 0.31102 Hz and 0.62205 Hz, respectively.

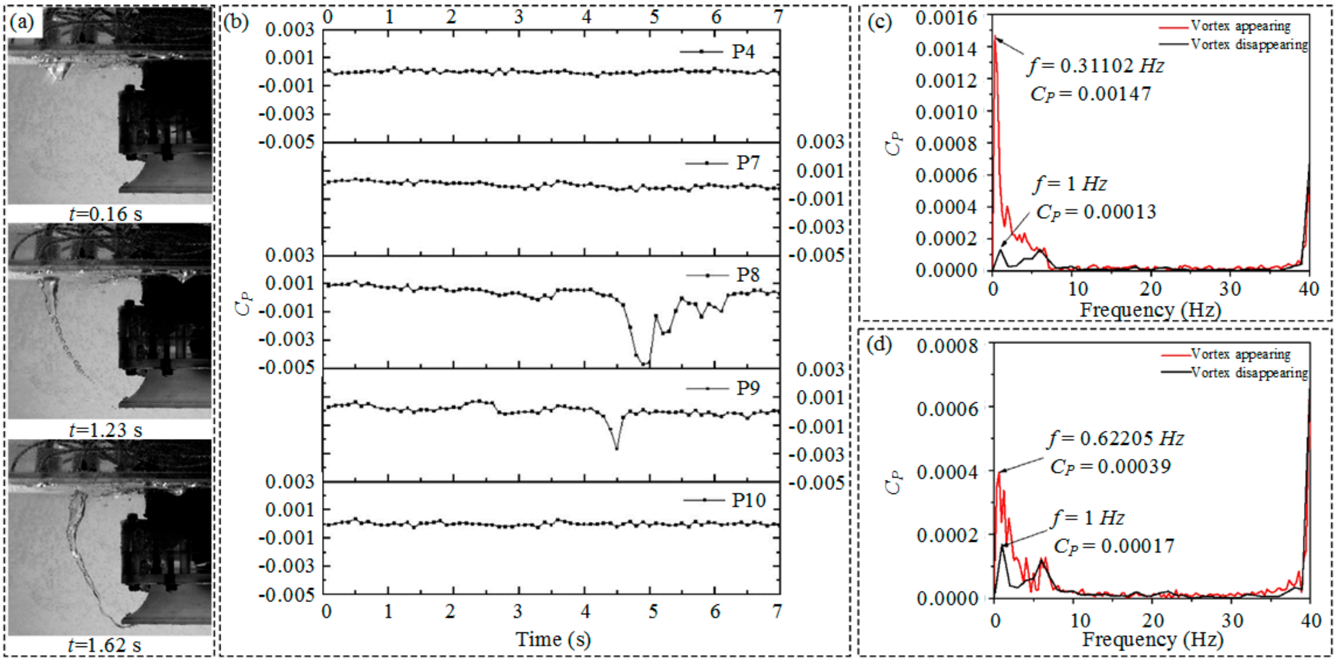

Figure 11. Pressure pulsation evolution of air entrainment. (**a**) Air entrainment process; (**b**) Time domain of monitoring points; (**c**,**d**) Spectrograms of vortexes and no vortexes. (Reprinted with permission from Ref. [89]. 2020, Elsevier).

According to the findings, pressure difference was the most critical component in the gas entrainment of the vortex, which was linked to the energy transition of the vortex formation, and pressure pulsation was the primary source of vortex-generated vibration [90,91]. A significant study direction was setting up a surface vortex's energy-pressure coupling model. Furthermore, the mechanism of pressure pulsation produced by differences in density, size, and volume of other material phases has to be considered. Hence, it is crucial to explore energy transition models of three-phase vortexes employing additional solid particle phases and the internal link between typical flow pattern transition state and pressure pulsation.

2.6. Vortex-Induced Vibration

The formation of vortices will result in gas entrainment phenomena. Due to the inherent instability of vortices, reactive fluctuations and high-frequency vortex-induced vibration (VIV) will occur, potentially causing damage to machinery and structures [92–94]. The excitation forces acting on the flow channels are challenging to calculate. The fluid–solid coupling vibration responses of flow channels under liquid impact become nonlinear. As a result, dynamic aspects of vortex-induced vibration, including the vibration responses and natural frequencies, must be studied.

Zhang [95] employed a wavelet-decomposition algorithm to discuss random vibration data. The method isolates key liquid constituents and derives abnormal spectral-energy distributions produced via pure-fluid vortex and impurity. Takács [96] performed real-time discussions of vortex-induced vibration signals using a cumulative sum control graph. For the most part, the measure shows a little modest vibration (± 0.5 ms^{-2}), and only a tiny amount of impurity change can be seen. Yenus [97] investigated the mechanisms of the sensor locations, impurity-phase depths, and sound signals. Recently, Li [98] studied the fluid-induced vibration characters and found that the signals had random components, especially in larger flows, showing an apparent step-increasing and diminishing characteristic.

Current research on vortex-induced vibration mainly focuses on two-phase flow shock, frequency characteristics, and energy flow propagation law, according to the study above [99]. Most studies had overlooked complicated boundary constraints, flow characteristics, and complex effects such as fluid, so vortex-induced vibration dynamic models were created to simplify, causing an error in the turbine operation in the process of impact vibration measurement. The multiphase flow with complex constraint boundary vortex-induced vibration response modeling technology and method were also flawed [100–102]. As a result, improving dynamic modeling technology and the propagating mechanisms of vortex-induced vibration at complicated boundary restrictions is critical.

3. Detection and Control of Gravitational Surface Vortex

3.1. Vortex-Induced Vibration Detection

The formation of a surface vortex causes a significant shift in drainage pressure pulsation, resulting in nonlinear impact vibration [100–103]. Real-time state identification of surface vortices utilizing vortex-induced vibration signals is a demanding task. The data capture of vibration signals in the industrial field environment is prone to high-frequency interference. These interfering problems make developing distortion-identifying methods for fluid-induced vibration signals extremely challenging. Therefore, basic or single signal-processing methods are insufficient to satisfy the criteria, and fluid-induced vibration signals must be optimized and integrated according to their properties.

Tan [48] proposed vibration-distortion detection techniques to recognize drainage states, providing a valuable reference for identifying flow states. Tan [104] presented a neural-network method to identify vortex states, and the accurate detection accuracy of the vortex-sucked impurity state can reach more than 96%. Chakraborty [105] utilized the CCD cameras to observe the sucking process of the slag and found that as flow rates increased, lots of solid impurities flowed into the lower equipment, and precision needed to be enhanced.

The effectiveness of the vibration detection system was closely linked to the real-time detection and precision of fluid-induced vibration signals. Without a doubt, the knowledge offered above is valuable. On the other hand, the intrinsic relationship between the surface vortex-induced vibration's physical evolution determines the signal detection algorithms' prosperity. The main goal is to develop a signal detection system that can recognize transition states of surface vortexes according to vortex hydrodynamic parameters.

The vortex-induced vibration detecting technologies have various advantages, such as investment costs, product qualities, and identification accuracies. (1) Using amplitude differences of vibration signals, the vibration detection techniques will analyze and observe the flow situation in the vortex formation process. (2) The monitoring sensors will be put in a remote location away from industrial environments to guarantee useful life and hydroelectric energy conversion rate. (3) The sensing platforms are easy to set up and service and do not need modifications to current hydraulic devices. (4) The equipment has a low production cost and is simple to popularize.

3.2. Suppression Control of Gravitational Surface Vortex

At the entrance of a hydropower station, the powerful, turbulent vortex near the intake will disrupt the inlet structure's regular operation. The vortex-induced vibration enters the hydraulic system, reducing turbine performance. In light of the issues above, it is critical to manage the formation of the surface vortex and avoid high-impact vibration, which causes significant equipment economic loss.

In recent years, the regulation of gravitational surface vortex formation in hydropower facilities has advanced significantly, yielding impressive results. The critical submerged depth control approach [106] is the most common method to prevent vortex formation during turbine operation. The shape of the vortex channel is modified to reduce the VIV by utilizing a device that prevents rotation and eliminates the vortex. Studying vortex dynamics must increase the control's efficacy and the device's dependability regardless of the approach used to regulate the vortex formation.

The so-called critical inundation depth control method involves keeping the water level in the reservoir or equipment above the critical inundation depth, which prevents the upper surface vortex from forming. This strategy, however, comes at the expense of hydropower energy conversion in actual hydropower turbine operation. As a result, the primary focus of future study will be on how to reduce the critical submerged depth of the surface vortex while maintaining the energy conversion rate of the hydropower station turbine unit.

Controlling the vortex generation by altering structures of the vortex passage using a device that prevents and eliminates vortex formation is a hot issue. This device does not require a significant change to the original water conservancy equipment. It is widely used in hydropower stations and other water conservancy projects due to its ease of installation and maintenance, long service life, good stability, sound economic benefits, and other advantages. This method fundamentally reduces the product to critical height, eliminates the entrained phenomenon, and reduces the strength of the vortex-induced vibration, thus improving the energy conversion rate.

Many academics have conducted experiments to better analyze and anticipate the effects of anti-vortex devices on input flows. Anti-eddy current devices of various sorts were tested, and the benefits and drawbacks of each device were documented [107]. Different methods may cause vortex dissipation in the presence of anti-vortex structures. The flow lines from the liquid surface to the intake are elongated using devices (e.g., Prosser disks and horizontal plates). Another device generates partial flow disruptions, causing turbulence, which prevents vortices from forming and allows them to dissipate (e.g., garbage racks and different types of perforated plates).

Wu [108] designed a circular cover plate mechanism to reduce the suction vortex created during the water pumping process. The circular cover plate is screwed between the apparatus's gravity water surface and the horn tube entrance. It has been discovered that increasing the disk size may remove the surface suction vortex. Khadem [109] investigated the vortex formation process of the anti-rotation device positioned at the reservoir's intake and discovered that, when compared to the Proser disk, the funnel reduced vorticity buildup and was more efficient when the immersion degree was greater. Reducing the immersion degree would limit its efficiency and eliminate vortex creation, making it a viable anti-vortex device option.

Son [68] suggested a simple and effective disc-type eddy current suppressor. The tank was emptied in 21 s with no suppressor and no tank rotation, as illustrated in Figure 12a. However, there was no dramatic shift in outlet flow in the suppressor case. Compared to a rotational tank without a suppressor, the time required for complete draining was reduced. In Figure 12b, the disk-type suppressor efficiently suppresses axial flow growth and vortex formation in the tank's center, and vorticity does not spread toward the center using suppressors. The developed disc damper efficiently restricted axial-momentum transmission at the vessel and effectively inhibited the Taylor vortex's expansion.

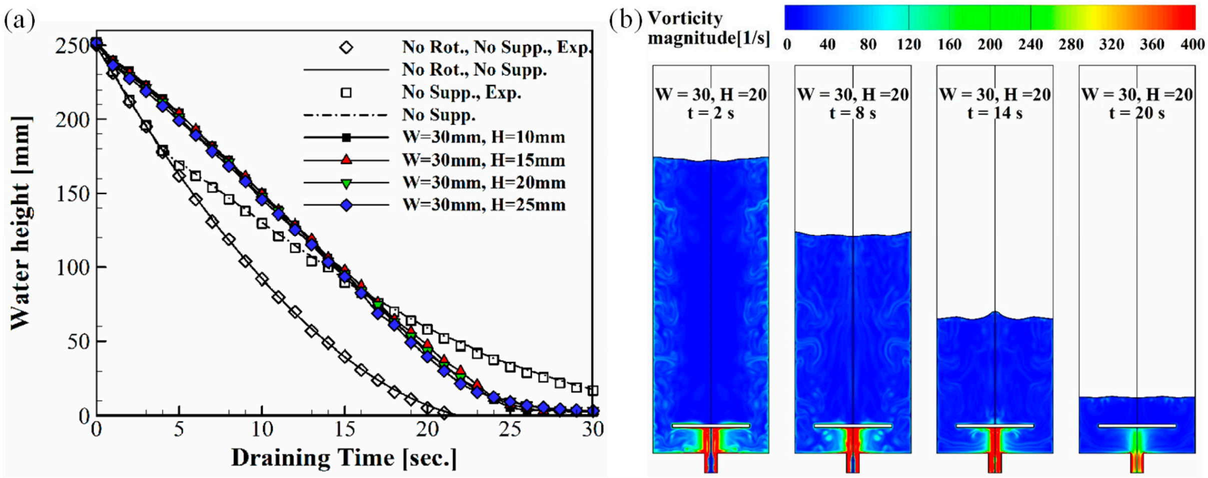

Figure 12. Comparison of the flow field with or without suppressor. (**a**) Variation of liquid height with different suppressor sizes. (**b**) Vorticity evolution with the suppressor. (Reprinted with permission from Ref. [68]. 2015, Springer Nature).

4. Research Trends and Prospects

The gravitational surface vortex is a typical occurrence in hydraulic engineering and detecting and suppressing its development process is critical for improving a hydropower turbine's operational stability and energy conversion rate. The study of the gravitational surface vortex has garnered increasing attention and interest from relevant scholars to improve the rate of utilization of hydropower energy and achieve clean and sustainable production.

The flow patterns and scale relationships of different shear layers in the Ekman boundary layer flow at a low Reynolds number have been studied. However, the vortex flow field may create a more complex flow layer structure in complex flow channel structures. It is necessary to analyze evolving relationships between a local turbulent vortex cluster and the Ekman number [53,54]. Another critical challenge is the analytical solution of the surface vortex considering the Ekman layer under turbulence conditions. The vital relationship between the evolution characteristics of the Ekman boundary layer (such as thickness, scale, etc.) and the critical transition state of the surface vortex should be analyzed. It can provide a theoretical reference for accurate vortex modeling at hydropower stations.

The existing theory of turbulence models tends to contain many assumptions and simplifications. One research direction is investigating the turbine equipment within the Ekman layer space-time multi-scale turbulence model [57]. Another direction is the 3D multi-scale modeling of a gravitational surface vortex. The Lattice Boltzmann (LB) approach has benefits in handling complicated interactions among physical issues at different scales, including multiphase flows, heat/mass transport, and chemical reactions [11,34], and it may be used to examine modeling technology for the surface vortex. As a result, more advanced multi-scale LB models are required to realize a multiphase coupling cross-scale flow, providing a reliable source for hydropower-turbine performance prediction.

The gravitational surface vortex is a complex turbulent phenomenon characterized by high curvature evolution and multiphase media coexistence. The complex flow channel structure is directly related to its multi-dimensional properties, such as the interface, vortex-core surface, and microscopic flow pattern [66,69]. Hence, it is necessary to develop 3D high-precision measured technologies of high-speed turbulent vortices with a complex spatial structure to achieve the quantitative analysis of the vortex core, a multiphase flow transformation mode, and the precise measurement of turbulent, vortex, dynamic characteristics across scales [70,72]. It is worth noting that the gas–liquid two-phase model of a hydropower station's surface vortex typically assumes fluid homogeneity and a no-slip mechanism. There are still many unanswered problems in researching a three-phase model that includes the particle phase [76]. The impact of solid-particle physical properties—such as form factor, density, size, and volume fraction on the vortex transport process of gravity surfaces—requires further investigation. Hence, investigating three-phase vortex models to evaluate head loss during hydropower plants is of great significance.

The intrinsic links between energy evolution and pressure pulsation in gas–liquid–solid flow require more research. As a result, establishing the energy-pressure coupling dynamic model of three-phase vortexes is an essential research direction. However, due to the complexity of coupling and the vast amount of calculation required, evaluating the impact of the solid particle phase transit on energy conversion and pressure pulsation remains a significant issue [87,88]. Moreover, a relevant gas–liquid–solid three-phase swirl experimental model should be built to confirm the correctness of the numerical model approach and to give technical support for hydropower-plant gravitational surface vortex prediction.

Due to complicated mechanical boundary limitations in the equipment flow passage of a hydropower plant, the fluid-structure coupling vibration response is very nonlinear. Existing VIV research ignores the impact of boundary limitations, pipeline features, and various media, resulting in random impact vibration measurement inaccuracies [103–105]. Exploring the multiphase fluid-structure coupling vibration dynamic model of the composite pipeline with complex boundary constraints and showing the essential relationship between vortex-induced vibration dynamic characteristics and the vortex formation process, is thus a meaningful direction. Moreover, optimizing flow-induced vibration signal processing algorithms is essential to extract nonlinear impact vibration mutation characteristics [106–111]. The above multi-source vibration data can supply research and development support for hydraulic vibration test systems in the hydropower field. Another research direction is designing and transforming internal resistance and vortex elimination devices for hydropower turbines. It can suppress the formation of vortices and reduce the suction ability of gas entrainment to avoid the generation of impact vibrations.

5. Conclusions

With the world's focus on clean, renewable energy, it is critical to boost hydroelectric energy conversion's efficiency and stability. This paper briefly discusses the surface vortex with hydrodynamic properties. A VIV signal recognized the formation condition of a surface vortex, and a vortex-suppression device was used to control the vortex. Future study directions of the gravitational surface vortex have then been prospected. Hydrodynamic features, formation detection, and vortex control have undoubtedly become research hotspots in the field of hydropower.

The dynamic evolution characteristics of surface vortices—such as the Ekman layer transport effect, heat/mass transfer, flow pattern tracing, and vortex-induced vibration—are systematically summarized. Adding the Ekman layer theory to vortex theory and numerical models can improve their accuracy, which is required to analyze surface vortices' dynamic properties. On the other hand, the analytical solution of Ekman-layer theory for powerful, turbulent vortices presents significant difficulties. Further research is needed to apply this theory to studying energy transfer and vorticity evolution in local vortex clusters and other transport phenomena. The next major step will be to build a high-precision, 3D, multi-scale modeling method of the gas–liquid–solid surface vortex.

Furthermore, pressure differences are the primary cause of gas entrainment, and pressure pulsation is the primary cause of vortex-induced vibration. Establishing the energy-pressure coupling dynamic model of surface vortices remains a significant difficulty. The above studies are expected to solve the pressure-pulsation mechanism caused by the different densities, sizes, and volumes of the particle phase in the complex gas–liquid–solid vortex-evolution process. The vibration dynamics modelling of three-phase flows with complex boundary constraints should be improved on this basis, considering the fluid-structure coupling boundary constraints under the actual operating conditions of hydropower stations. It can further reveal the essential relationship between the particle-flow pattern transition, pressure pulsation, and vortex-induced vibration.

The signal-processing method should be merged and improved according to the features of vortex-induced vibration signals to detect the critical state of the surface vortex in real time, increasing the success rate and stability of vibration detection. Effective procedures—including submerged depth control, blocking rotation, and the vortex-eliminating device—are used to regulate the creation of the surface vortex. Furthermore, by employing blocking spin and vortex elimination devices, the structure of the vortex passage can be altered, and vortex suppression management is a topic on which there is a strong focus. The external device suppression method can fundamentally lower the critical vortex height, reduce the phenomenon of gas or impurities sucked by the vortex, and decrease the intensity of the vortex-induced vibration, all of which have important practical implications for improving the hydropower energy-conversion rate.

The detection and control of gravitational surface vortex formation as a common water-conservation phenomenon in the operation of hydropower stations is vital for improving the hydropower energy-utilization rate and reducing damage to hydraulic equipment. However, its application process has some important challenges. This overview will aid potential scholars in rapidly grasping the overall topic of gravitational-surface vortex research. It can help identify research directions and critical technological issues.

Author Contributions: Conceptualization, G.Z. and W.X.; article identification, screening, retrieval, selection, and analysis, G.Z. and L.L.; formal analysis and investigation, G.Z. and Z.G.; writing—original draft preparation, G.Z. and L.L.; tables and figures generation, G.Z. and B.L.; review and editing, G.Z., W.X., Y.T., C.W., Q.L. and Z.G.; supervision, L.L. funding acquisition, L.L. All authors have read and agreed to the published version of the manuscript.

Funding: This work was supported in part by the Zhejiang Provincial Natural Science Foundation under Grant No. LQ23E050017; Zhejiang Province Postdoctoral Scientific Research Preferred Funding Project under Grant No. ZJ2022068; Open Foundation of the State Key Laboratory of Fluid Power and Mechatronic Systems under Grant No. GZKF-202125.

Data Availability Statement: Not applicable.

Conflicts of Interest: The authors declare that they have no conflict of interest.

References

1. Rostami, A.B.; Armandei, M. Renewable energy harvesting by vortex-induced motions: Review and benchmarking of technologies. *Renew. Sustain. Energy Rev.* **2017**, *70*, 193–214. [CrossRef]
2. Waseem, A.; Ali, U.; Shi, J.M.; Yuan, K.; Qina, M.; Zou, R.Q. Phase change material-integrated latent heat torage systems for sustainable energy solutions. *Energy Environ. Sci.* **2021**, *14*, 42–68.
3. Zhang, Y.N.; Liu, K.H.; Xian, H.Z.; Du, X.Z. A review of methods for vortex identification in hydroturbines. *Renew. Sustain. Energy Rev.* **2018**, *81*, 1269–1285. [CrossRef]
4. Li, L.; Lu, B.; Xu, W.X.; Gu, Z.H.; Yang, Y.S.; Tan, D.P. Multiphase coupling transport evolution mechanism of the free sink vortex. *Acta Phys. Sin.* 2023, *in press*.
5. Zhu, D.; Tao, R.; Xiao, R.F.; Pan, L.T. Solving the runner blade crack problem for a Francis hydro-turbine operating under condition-complexity. *Renew. Energy* **2020**, *149*, 298–320. [CrossRef]
6. Li, L.; Xu, W.X.; Tan, Y.F.; Yang, Y.S.; Yang, J.G.; Tan, D.P. Fluid-induced vibration evolution mechanism of multiphase free sink vortex and the multi-source vibration sensing method. *Mech. Syst. Signal Process.* 2023, *in press*.
7. Saleem, A.S.; Cheema, T.A.; Ahmad, S.M.; Chatta, J.A.; Akbar, B.; Park, C.W. Parametric study of single-stage gravitational water vortex turbine with cylindrical basin. *Energy* **2020**, *200*, 117464. [CrossRef]
8. Zhang, B.; Guo, X.J. Prospective applications of Ranque-Hilsch vortex tubes to sustainable energy utilization and energy efficiency improvement with energy and mass separation. *Renew. Sustain. Energy Rev.* **2018**, *89*, 135–150. [CrossRef]
9. Li, L.; Lu, B.; Xu, W.X.; Wang, C.Y.; Wu, J.F.; Tan, D.P. Dynamic behaviors of multiphase vortex-induced vibration for hydropower energy conversion. *Energy* 2023, *in press*.

10. Yang, J.J.; He, E.M. Coupled modeling and structural vibration control for floating offshore wind turbine. *Renew. Energy* **2020**, *157*, 678–694. [CrossRef]
11. Li, L.; Fang, H.; Yin, Z.C.; Wang, T.; Wang, R.H.; Fan, X.H.; Zhao, L.J.; Tan, D.P.; Wan, Y.H. Lattice Boltzmann method for fluid-thermal systems: Status, hotspots, trends and outlook. *IEEE Access* **2020**, *8*, 27649–27675. [CrossRef]
12. Ge, J.Q.; Ren, Y.L.; Li, C.; Li, Z.A.; Yan, S.T.; Tang, P.; Xu, X.S.; Wang, Q. Ultrasonic coupled abrasive jet polishing (UC-AJP) of glass-based micro-channel for micro-fluidic chip. *Int. J. Mech. Sci.* 2023, *in press*. [CrossRef]
13. Goyal, R.; Gandhi, B.K.; Cervantes, M.J. PIV measurements in Francis turbine—A review and application to transient operations. *Renew. Sustain. Energy Rev.* **2018**, *81*, 2976–2991. [CrossRef]
14. Li, L.; Gu, Z.H.; Xu, W.X.; Tan, Y.F.; Fan, X.H.; Tan, D.P. Mixing mass transfer mechanism and dynamic control of gas-liquid-solid multiphase flow based on VOF-DEM coupling. *Energy* 2023, *in press*.
15. Ezure, T.; Kimura, N.; Miyakoshi, H.; Kamide, H. Experimental investigation on bubble characteristics entrained by surface vortex. *Nucl. Eng. Des.* **2011**, *241*, 4575–4584. [CrossRef]
16. Sun, Z.; Jin, H.; Gu, J. Studies on the online intelligent diagnosis method of undercharging sub-health air source heat pump water heater. *Appl. Therm. Eng.* **2020**, *169*, 114957. [CrossRef]
17. Liu, Y.; Chen, W.; Zhang, W.; Ma, C.Q.; Chen, H.X.; Xiong, Y.F.; Yuan, R.; Tang, J.; Chen, P.; Hu, W.; et al. Visible and online detection of near-infrared optical vortices via nonlinear photonic crystals. *Adv. Opt. Mater.* **2021**, *10*, 2101098. [CrossRef]
18. Wei, J.J.; Li, F.C.; Yu, B.; Kawaguchi, Y. Swirling flow of a viscoelastic fluid with free surface: Part I-Experimental analysis of vortex motion by PIV. *J. Fluids Eng.-Trans. ASME* **2006**, *128*, 813–819. [CrossRef]
19. Zhao, Y.Z.; Gu, Z.L.; Yu, Y.Z.; Li, Y.; Feng, X. Numerical analysis of structure and evolution of free water vortex. *J. Xi'an Jiaotong Univ.* **2003**, *37*, 85–88.
20. Li, H.X.; Wang, Q.; Lei, H. Mechanism analysis of free-surface vortex formation during steel Teeming. *ISIJ Int.* **2014**, *54*, 1592–1600. [CrossRef]
21. Tan, Y.F.; Ni, Y.S.; Wu, J.F.; Li, L.; Tan, D.P. Machinability evolution of gas-liquid-solid three-phase rotary abrasive flow finishing. *Int. J. Adv. Manuf. Technol.* **2023**, *in press*.
22. Trefethen, L.M.; Bilger, R.W.; Fink, P.T. The bathtub vortex in the southern hemisphere. *Nature* **1965**, *207*, 1084–1085. [CrossRef]
23. Arab, A.; Javadi, M.; Anbarsooz, M.; Moghiman, M. A numerical study on the aerodynamic performance and the self-starting characteristics of a Darrieus wind turbine considering its moment of inertia. *Renew. Energy* **2017**, *107*, 298–311. [CrossRef]
24. Hecker, G.E. Model-prototype comparison of free surface vertices. *J. Hydraul. Div.* **1981**, *107*, 1243–1259. [CrossRef]
25. Yin, Z.C.; Ni, Y.S.; Li, L.; Wang, T.; Wu, J.F.; Li, Z.; Tan, D.P. Numerical modelling and experimental investigation of a two-phase sink vortex and its fluid-solid vibration characteristics. *J. Zhejiang Univ.-Sci. A.* 2022; *in press*.
26. Wang, J.X.; Gao, S.B.; Tang, Z.J.; Tan, D.P. A context-aware recommendation system for improving manufacturing process modeling. *J. Intel. Manuf.* 2021; *in press*.
27. Jeong, J.T. Free-surface deformation due to spiral flow owing to a source/sink and a vortex in stokes flow. *Theor. Comput. Fulid Dyn.* **2012**, *26*, 93–103. [CrossRef]
28. Li, M.; Mustahsan, V.M.; He, G.Y.; Tavernier, F.B.; Singh, G.; Boyce, B.F.; Khan, F.; Kao, I. Classification of soft tissue sarcoma specimens with raman spectroscopy as smart sensing technology. *Cyborg Bionic Syst.* **2021**, *2021*, 9816913. [CrossRef]
29. Wang, Q.; Wang, L.Y.; Li, H.X.; Jiang, J.W.; Zhu, X.W.; Guo, Z.C.; He, J.C. Suppression mechanism and method of vortex during steel teeming process in ladle. *Acta Metall. Sin.* **2018**, *7*, 959–968.
30. Du, X.Z.; Zhang, M.; Chang, H.; Wang, Y.; Yu, H. Micro windmill piezoelectric energy harvester based on vortex-induced vibration in tunnel. *Energy* **2022**, *238*, 121734. [CrossRef]
31. Devenport, W.; Rife, M.; Liapis, S. The structure and development of a wing-tip vortex. *J. Fluid Mech.* **1996**, *312*, 67–106. [CrossRef]
32. Weisberg, A.Y.; Kevrekidis, I.G.; Smits, A.J. Delaying transition in tayor-couette flow with axial motion of the inner cylinder. *J. Fluid Mech.* **1997**, *348*, 141–151. [CrossRef]
33. Lewellen, W.S. A Solution for three-dimensional vortex flows with strong circulation. *J. Fluid Mech.* **1962**, *14*, 420–433. [CrossRef]
34. Tyvand, P.A.; Haugen, K.B. An impulsive bathtub vortex. *Phys. Fluids* **2005**, *17*, 062105. [CrossRef]
35. Tan, D.P.; Zhang, L.B.; Ai, Q.L. An embedded self-adapting network service framework for networked manufacturing system. *J. Intell. Manuf.* **2019**, *30*, 539–556. [CrossRef]
36. Zheng, M.R.; Han, D.; Peng, T. Numerical investigation on flow induced vibration performance of flow-around structures with different angles of attack. *Energy* **2022**, *244*, 122607. [CrossRef]
37. Tan, D.P.; Ji, S.M.; Fu, Y.Z. An improved soft abrasive flow finishing method based on fluid collision theory. *Int. J. Adv. Manuf. Technol.* **2016**, *85*, 1261–1274. [CrossRef]
38. Aboelkassem, Y.; Vatistas, G.H.; Esmail, N. Viscous dissipation of Rankine vortex profile in zero meridional flow. *Acta Mech. Sin.* **2005**, *21*, 550–556. [CrossRef]
39. Wu, H.P.; Li, L.; Chai, G.Z.; Song, F.; Kitamura, T. Three-dimensional thermal weight function method for the interface crack problems in bimaterial structures under a transient thermal loading. *J. Therm. Stress.* **2016**, *39*, 371–385. [CrossRef]
40. Huang, X.Y.; Cheng, W.J.; Zhong, W.; Li, X. Development of new pressure regulator with flowrate-amplification using vacuum ejector. *Vacuum* **2017**, *144*, 172–182. [CrossRef]
41. Odgaard, A.J. Free-surface air core vortex. *J. Hydraul. Eng.* **1986**, *112*, 610–620. [CrossRef]
42. Odgaard, A.J. Discussion of "Free-surface air core vortex". *J. Hydraul. Eng.* **1988**, *114*, 449–452.

43. Sun, Z.; Jin, H.; Xu, Y. Severity-insensitive fault diagnosis method for heat pump systems based on improved benchmark model and data scaling strategy. *Energy Build.* **2022**, *256*, 111733. [CrossRef]
44. Wang, H.; Kan, J.C.; Zhang, X.; Gu, C.Y.; Yang, Z. Pt/CNT micro-nanorobots driven by glucose catalytic decomposition. *Cyborg Bionic Syst.* **2021**, *2021*, 9876064. [CrossRef]
45. Ghani, I.A.; Sidik, N.A.C.; Kamaruzaman, N. Hydrothermal performance of microchannel heat sink: The effect of channel design. *Int. J. Heat Mass Transf.* **2017**, *107*, 21–44. [CrossRef]
46. Tan, D.P.; Ji, S.M.; Li, P.Y.; Pan, X.H. Development of vibration style ladle slag detection method and the key technologies. *Sci. China-Technol. Sci.* **2010**, *53*, 2378–2387. [CrossRef]
47. Wang, Y.Y.; Zhang, Y.L.; Tan, D.P.; Zhang, Y.C. Key technologies and development trends in advanced intelligent sawing equipments. *Chin. J. Mech. Eng.* **2021**, *34*, 30. [CrossRef]
48. Tan, D.P.; Zhang, L.B. A WP-based nonlinear vibration sensing method for invisible liquid steel slag detection. *Sens. Actuators B-Chem.* **2014**, *202*, 1257–1269. [CrossRef]
49. Dolan, S.R.; Oliveira, E.S. Scattering by a draining bathtub vortex. *Phys. Rev. D* **2013**, *87*, 124038. [CrossRef]
50. Fan, X.T.; Guo, K.; Wang, Y. Toward a high performance and strong resilience wind energy harvester assembly utilizing flow-induced vibration: Role of hysteresis. *Energy* **2022**, *251*, 123921. [CrossRef]
51. Scheeler, M.W.; Van Rees, W.M.; Kedia, H.; Kleckner, D.; Irvine, W.T.M. Complete measurement of helicity and its dynamics in vortex tubes. *Science* **2017**, *357*, 487–490. [CrossRef] [PubMed]
52. Zhang, K.K.; Chan, K.H.; Liao, X.H. Asymptotic theory of resonant flow in a spheroidal cavity driven by latitudinal libration. *J. Fluid Mech.* **2012**, *692*, 420–445. [CrossRef]
53. Andersen, A.; Bohr, T.; Stenum, B.; Rasmussen, J.J.; Lautrup, B. The bathtub vortex in a rotating container. *J. Fluid Mech.* **2006**, *556*, 121–146. [CrossRef]
54. Chen, Y.C.; Huang, S.L.; Li, Z.Y.; Chang, C.C.; Chu, C.C. A bathtub vortex under the influence of a protruding cylinder in a rotating tank. *J. Fluid Mech.* **2013**, *733*, 134–157. [CrossRef]
55. Son, J.H.; Park, I.S. Prevention of air entrainment during liquid draining using disc-type vortex suppressor. *J. Mech. Sci. Technol.* **2018**, *32*, 4675–4682. [CrossRef]
56. Park, I.S.; Sohn, C.H. Experimental and numerical study on air cores for cylindrical tank draining. *Int. Commun. Heat Mass Transf.* **2011**, *38*, 1044–1049. [CrossRef]
57. Yokoyama, N.; Maruyama, Y.; Mizushima, J. Origin of the bathtub vortex and its formation mechanism. *J. Phys. Soc. Jpn.* **2012**, *81*, 074401. [CrossRef]
58. Kim, D.; Kim, D. Free-surface vortex formation and aeration by a submerged rotating disk. *Chem. Eng. Sci.* **2021**, *243*, 116787. [CrossRef]
59. Lamont, J.C.; Scott, D.S. An eddy cell model of mass transfer into the surface of a turbulent liquid. *AIChE J.* **1970**, *16*, 513–519. [CrossRef]
60. Morales, R.D.; Davila-Maldonado, O.; Calderon, I.; Morales-Higa, K. Physical and mathematical models of vortex flows during the last stages of steel draining operations from a ladle. *ISIJ Intern.* **2013**, *53*, 782–791. [CrossRef]
61. Aravind, G.P.; Deepu, M. Numerical study on convective mass transfer enhancement by lateral sweep vortex generators. *Int. J. Heat Mass Transf.* **2017**, *115*, 809–825. [CrossRef]
62. Nazir, K.; Sohn, C.H. Effect of water temperature on air-core generation and disappearance during draining. *J. Mech. Sci. Technol.* **2018**, *32*, 703–708. [CrossRef]
63. Tan, D.P.; Li, L.; Yin, Z.C.; Li, D.F.; Zhu, Y.L.; Zheng, S. Ekman boundary layer mass transfer mechanism of free sink vortex. *Int. J. Heat Mass Transf.* **2020**, *150*, 119250. [CrossRef]
64. Monji, H.; Shinozaki, T.; Kamide, H.; Sakai, T. Effect of experimental conditions on gas core length and downward velocity of free surface vortex in cylindrical vessel. In Proceedings of the 16th International Conference on Nuclear Engineering, Orlando, FL, USA, 11–15 May 2008.
65. Tahershamsi, A.; Rahimzadeh, H.; Monshizadeh, M.; Sarkardeh, H. An experimental study on free surface vortex dynamics. *Meccanica* **2018**, *53*, 3269–3277. [CrossRef]
66. Ruan, Y.W.; Yao, Y.; Shen, S.Y. Physical and mathematical simulation of surface-free vortex formation and vortex prevention design during the end of casting in tundish. *Steel Res. Int.* **2020**, *91*, 1900616. [CrossRef]
67. Mulligan, S.; De Cesare, G.; Casserly, J.; Sherlock, R. Understanding turbulent free-surface vortex flows using a Taylor-Couette flow analogy. *Sci. Rep.* **2018**, *8*, 824. [CrossRef] [PubMed]
68. Son, J.H.; Sohn, C.H.; Park, I.S. Numerical study of 3-D air core phenomenon during liquid draining. *J. Mech. Sci. Technol.* **2015**, *29*, 4247–4257. [CrossRef]
69. Wu, P.F.; Munoz, D.H.; Constantinescu, G.; Qian, Z.D. Two-phase flow DES and URANS simulations of pump-intake bay vortices. *J. Hydraul. Res.* **2020**, *58*, 120–132. [CrossRef]
70. Yang, M.; Liu, S.; Xu, W.H. Numerical and experimental studies of an oil slick recovery method that uses a free surface vortex. *ACS Omega* **2020**, *5*, 31332–31341. [CrossRef]
71. Tan, D.P.; Li, L.; Zhu, Y.L.; Zheng, S.; Yin, Z.C.; Li, D.F. Critical penetration condition and Ekman suction–extraction mechanism of a sink vortex. *J. Zhejiang Univ.-Sci. A.* **2019**, *20*, 61–72. [CrossRef]

72. Duinmeijer, A.; Clemens, F. An experimental study on the motion of buoyant particles in the free-surface vortex flow. *J. Hydraul. Res.* **2021**, *59*, 947–962. [CrossRef]
73. Duinmeijer, S.P.A.; Moreno-Rodenas, A.M.; Lepot, M.; van Nieuwenhuizen, C.; Meyer, I.; Clemens, F.H.L.R. A simple measuring set-up for the experimental determination of the dynamics of a large particle in the 3D velocity field around a free surface vortex. *Flow Meas. Instrum.* **2019**, *65*, 52–64. [CrossRef]
74. Xie, H.Y.; Cao, Y.; Qin, F.H.; Luo, X.S. The slip effect of micro-droplets in Rankine vortex. *Sci. Sin. Phys. Mech. Astron.* **2017**, *47*, 124702-1–124702-9. [CrossRef]
75. Li, L.; Qi, H.; Yin, Z.C.; Li, D.F.; Zhu, Z.L.; Tangwarodomnukun, V.; Tan, D.P. Investigation on the multiphase sink vortex Ekman pumping effects by CFD-DEM coupling method. *Powder Technol.* **2019**, *360*, 462–480. [CrossRef]
76. Wei, N.; Sun, W.T.; Meng, Y.F.; Liu, A.Q.; Zhao, J.Z.; Zhou, S.W.; Zhang, L.H.; Li, Q.P. Multiphase non equilibrium pipe flow behaviors in the solid fluidization exploitation of marine natural gas hydrate reservoir. *Energy Sci. Eng.* **2019**, *6*, 760–782. [CrossRef]
77. Zheng, X.J.; Feng, S.J.; Wang, P. Modulation of turbulence by saltating particles on erodible bed surface. *J. Fluid Mech.* **2021**, *918*, A16. [CrossRef]
78. Kang, Q.Q.; He, D.P.; Zhao, N.; Feng, X.; Wang, J.T. Hydrodynamics in unbaffled liquid-solid stirred tanks with free surface studied by DEM-VOF method. *Chem. Eng. J.* **2020**, *386*, 122846-1–122846-17. [CrossRef]
79. Yasuda, T.; Kawahara, G.; van Veen, L.; Kida, S. A vortex interaction mechanism for generating energy and enstrophy fluctuations in high-symmetric turbulence. *J. Fluid Mech.* **2019**, *874*, 639–676. [CrossRef]
80. Osawa, K.; Minamoto, Y.; Shimura, M.; Tanahashi, M. Voronoi analysis of vortex clustering in homogeneous isotropic turbulence. *Phys. Fluids* **2021**, *33*, 035138. [CrossRef]
81. Song, S.L.; Zhao, Q.B.; Chong, D.T.; Chen, W.X.; Yan, J.J. Numerical simulation of vortex in residual heat removal system during mid-loop operation. *Nucl. Eng. Des.* **2018**, *337*, 428–438. [CrossRef]
82. Naderi, V.; Farsadizadeh, D.; Lin, C.; Gaskin, S. A 3D Study of an Air-Core Vortex Using HSPIV and Flow Visualization. *Arab. J. Sci. Eng.* **2019**, *44*, 8573–8584. [CrossRef]
83. Zheng, G.A.; Li, L.; Li, Q.H.; Gu, Z.H.; Xu, W.X.; Lu, B. Fluid-solid coupling-based vibration generation mechanism of the multiphase vortex. *Processes* 2023, *in press*.
84. Ali, Q.S.; Kim, M.H. Power conversion performance of airborne wind turbine under unsteady loads. *Renew. Sustain. Energy Rev.* **2022**, *153*, 111798. [CrossRef]
85. Toshio, F. Cyborg and bionic systems: Signposting the future. *Cyborg Bionic Syst.* **2020**, *2020*, 1310389.
86. Qian, Z.D.; Wu, P.F.; Guo, Z.W.; Huai, W.X. Numerical simulation of air entrainment and suppression in pump sump. *Sci. China-Technol. Sci.* **2017**, *59*, 1847–1855. [CrossRef]
87. Skerlavaj, A.; Skerget, L.; Ravnik, J.; Lipej, A. Predicting Free-Surface Vortices with Single-Phase Simulations. *Eng. Appl. Comput. Fluid Mech.* **2014**, *8*, 193–210. [CrossRef]
88. Ezure, T.; Ito, K.; Tanaka, M.; Ohshima, H.; Kameyama, Y. Experiments on gas entrainment phenomena due to free surface vortex induced by flow passing beside stagnation region. *Nucl. Eng. Des.* **2019**, *350*, 90–97. [CrossRef]
89. Zhang, D.; Jiao, W.X.; Cheng, L.; Xia, C.Z.; Zhang, B.W.; Luo, C.; Wang, C. Experimental study on the evolution process of the roof-attached vortex of the closed sump. *Renew. Energy* **2020**, *164*, 1029–1038. [CrossRef]
90. Wang, F.J.; Zhang, L.; Zhang, Z.M. Analysis on pressure fluctuation of unsteady flow in axial-flow pump. *J. Hydraul. Eng.* **2007**, *38*, 1003–1009.
91. Song, X.J.; Liu, C. Experimental investigation of pressure pulsation induced by the floor-attached vortex in an axial flow pump. *Adv. Mech. Eng.* **2019**, *11*, 1687814019838708. [CrossRef]
92. Yang, F.; Liu, C. Numerical and Experimental Investigations of Vortex Flows and Vortex Suppression Schemes in the Intake Passage of Pumping System. *Adv. Mech. Eng.* **2015**, *7*, 547086. [CrossRef]
93. Favrel, A.; Muller, A.; Landry, C.; Yamamoto, K.; Avellan, F. Study of the vortex-induced pressure excitation source in a Francis turbine draft tube by particle image velocimetry. *Exp. Fluids* **2015**, *56*, 215. [CrossRef]
94. Baghlani, A.; Khayat, M.; Dehghan, S.M. Free vibration analysis of FGM cylindrical shells surrounded by Pasternak elastic foundation in thermal environment considering fluid-structure interaction. *Appl. Math. Model.* **2019**, *78*, 550–575. [CrossRef]
95. Zhang, Q.; Wang, J.; Zhang, Y.Z.; Xu, G.G. Numerical simulation and manifold learning for the vibration of molten steel draining from a ladle. *J. Vibroeng.* **2013**, *15*, 549–557.
96. Takacs, G.; Ondrejkovic, K.; Hulko, G. A low-cost non-invasive slag detection system for continuous casting. *IFAC Pap.* **2017**, *50*, 438–445. [CrossRef]
97. Yenus, J.; Brooks, G.; Dunn, M.; Kadam, R. Application of vibration and sound signals in monitoring iron and steelmaking processes. *Ironmak. Steelmak.* **2020**, *47*, 178–187. [CrossRef]
98. Li, L.; Tan, D.P.; Yin, Z.C.; Wang, T.; Fan, X.H.; Wang, R.H. Investigation on the multiphase vortex and its fluid-solid vibration characters for sustainability production. *Renew. Energy* **2021**, *175*, 887–909. [CrossRef]
99. Alligne, S.; Nicolet, C.; Beguin, A.; Landry, C.; Gomes, J.; Avellan, F. Hydroelectric System Response to Part Load Vortex Rope Excitation. *IOP Conf. Ser.-Earth Environ. Sci.* **2016**, *49*, 052002. [CrossRef]
100. Tan, D.P.; Li, L.; Zhu, Y.L.; Zheng, S.; Ruan, H.J.; Jiang, X.Y. An embedded cloud database service method for distributed industry monitoring, IEEE Trans. *Ind. Inform.* **2018**, *14*, 2881–2893. [CrossRef]

101. Yang, Y.; Bashir, M.; Li, C.; Michailides, C.; Wang, J. Mitigation of coupled wind-wave-earthquake responses of a 10 MW fixed-bottom offshore wind turbine. *Renew. Energy* **2020**, *157*, 1171–1184. [CrossRef]
102. Li, P.Y.; Zou, F.X. Application of HMM theory in vibration detection method of slag in continuous casting. *Metall. Ind. Autom.* **2005**, *1*, 14–18.
103. Zhang, B.S.; Li, B.Y.; Fu, S.; Mao, Z.Y.; Ding, W.J. Vortex-Induced Vibration (VIV) hydrokinetic energy harvesting based on nonlinear damping. *Renew. Energy* **2022**, *195*, 1050–1063. [CrossRef]
104. Tan, D.P.; Li, P.Y.; Ji, Y.X.; Wen, D.H.; Li, C. SA-ANN-based slag carry-over detection method and the embedded WME platform. *IEEE Trans. Ind. Electron.* **2013**, *60*, 4702–4713. [CrossRef]
105. Chakraborty, A.; Ghose, J.; Chakraborty, S.; Chakraborty, B. Vision-based detection system of slag flow from ladle to tundish with the help of the detection of undulation of slag layer of the tundish using an image analysis technique. *Ironmak. Steelmak.* **2021**, *49*, 10–15. [CrossRef]
106. Wang, C.; Hu, B.; Zhu, Y.; Wang, X.L.; Luo, C.; Cheng, L. Numerical Study on the Gas-Water Two-Phase Flow in the Self-Priming Process of Self-Priming Centrifugal Pump. *Processes* **2019**, *7*, 330. [CrossRef]
107. Taghvaei, S.M.; Roshan, R.; Safavi, K.H.; Sarkardeh, H. Anti-vortex structures at hydropower dams. *Int. J. Phys. Sci.* **2012**, *7*, 5069–5077. [CrossRef]
108. Wu, P.F.; Guo, Z.W.; Qian, Z.D.; Wang, Z.Y.; Chen, F. Numerical Simulation and Experiment on Free-surface Air-entraining Vortices in Pump Sump. *Trans. Chin. Soc. Agric. Mach.* **2018**, *49*, 120–125.
109. Khadem, B.; Najafabadi, S.H.G.; Sarkardeh, H. Numerical simulation of anti-vortex devices at water intakes. *Proc. Inst. Civ. Eng.-Water Manag.* **2018**, *171*, 18–29. [CrossRef]
110. Li, L.; Yang, Y.S.; Xu, W.X.; Lu, B.; Gu, Z.H.; Yang, J.G.; Tan, D.P. Advances in the multiphase vortex-induced vibration detection method and its vital technology for sustainable industrial production. *Appl. Sci.* **2022**, *12*, 8538. [CrossRef]
111. Li, L.; Tan, D.P.; Wang, T.; Yin, Z.C.; Fan, X.H.; Wang, R.H. Multiphase coupling mechanism of free surface vortex and the vibration-based sensing method. *Energy* **2021**, *216*, 119136. [CrossRef]